# Design of Metal Building Roof Purlins
# Including System Reliability Effects

S. Torabian, B.W. Schafer

**Design of Metal Building Roof Purlins Including System Reliability Effects**

S. Torabian, B.W. Schafer

## 1.      ABSTRACT

This report provides a framework to incorporate structural system reliability effects in the design of roof purlins in a typical metal building. Today every roof purlin is considered as a separate component and the effect of spatial variation in the demand loads and potential redistribution and load sharing in the roof system capacity are ignored in design. Component reliability is established by first-order reliability methods implemented through load and resistance factor design. Based on recent work in loading bearing cold-formed steel framing systems the load and resistance factor design framework is extended from components to systems through an additional resistance factor to account for system influence. An archetypical metal building is designed and selected for this study. Monte Carlo simulations of a segment of the metal building roof are performed with consideration of both randomness in the demands and capacity and employing geometric and material nonlinearity in the response model of the roof. The simulations indicate that the system effect in metal building roofs is beneficial, and increases in the design capacity when evaluated against demands may be appropriate. Sensitivity to the target reliability (allowed probability of failure), deflection limits, and modeling assumptions are observed and discussed. Preliminary factors to account for roof system reliability are provided.

## 2.      INTRODUCTION

In metal building design today every component in the building sees a separate design check. If any one component fails we predict the entire building fails. That is, we use component reliability to try to design the system. In the future one can readily imagine a more involved framework. Engineers establish the desired system reliability (i.e. desired system failure probability) and the reliability of a component matters only insofar as it influences the system. One approach to realize this vision, that allows current workflows to largely continue, would be to embed the influence of the system within the engineer's individual component checks – this approach is explored herein.

In today's design framework (e.g., ASCE7-16 for demand, AISI S100-16 for capacity) component reliability, $\beta$, is established through first-order second-moment reliability methods implemented through load and resistance factor design generally expressed as

$$\phi R_n \geq c \Sigma \gamma Q_n^* \tag{1}$$

where $\phi$ is the resistance factor, $R_n$ is the nominal strength of the component, $c$ is a factor that converts load demand to load effect (axial force, moment, etc.) and can be understood as the result of conducting a linear structural analysis, $\gamma$ is the load combination effect (e.g. 1.2 in 1.2D), and $Q_n^*$ is the nominal demand (e.g., D). The component reliability consistent, $\beta$, consistent with Figure 1 is established as

$$\beta = \frac{\ln\left(\frac{R}{Q}\right)_m}{\sigma_{\ln\left(\frac{R}{Q}\right)}} \tag{2a}$$

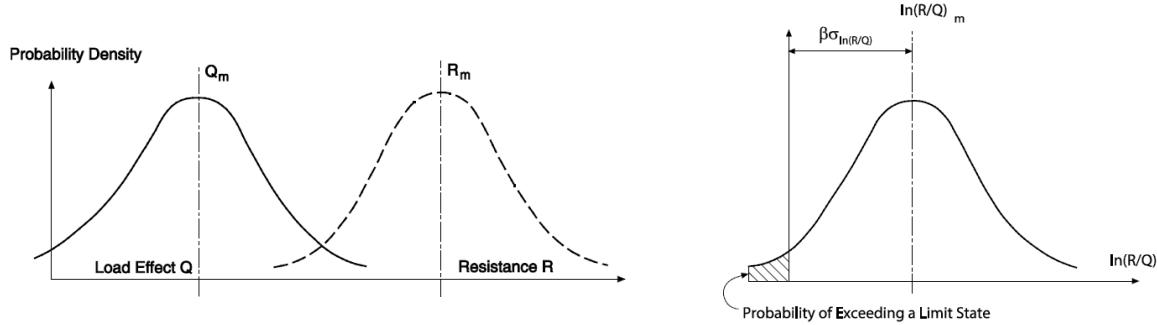$$\cong \frac{\ln(R_m/Q_m)}{\sqrt{V_R^2+V_Q^2}} \tag{2b}$$



Figure 1: Basic component reliability concepts (a) definition of the randomness $Q$ and $R$; (b) definition of the reliability index β (AISI 2016)

where $R$ and $Q$ are random variables, subscript $m$ denotes mean, and $\sigma$ standard deviation – $R_m$ is the mean resistance, $Q_m$ is the mean demand (load) <u>effect</u>, $V_R$ is the coefficient of variation for the resistance, and $V_Q$ is the coefficient of variation for the load effect. The mean factors are connected to the nominal values in Eq. (1) by:

$$R_m = M_m F_m P_m R_n \tag{3}$$

$$Q_m = c\Sigma B Q_n^* \tag{4}$$

where $M$, $F$, and $P$ are the material, fabrication, and professional factors where subscript $m$ refers to their mean values and $B$ is the bias factors between the nominal loads and the mean load. For the case where demand = capacity, substituting Eq. (1) into Eq. (3) we can see that $R_m$ may also be expressed as:

$$R_m = M_m F_m P_m (1/\phi) c\Sigma\gamma Q_n^* \tag{5}$$

Eq. (5) shows that the resistance factor, $\phi$, may be used to tune $R_m$ and as a result, $\beta$. Substitute Eq. (4) and (5) into (2b) for the direct expression.

For a system a direct approach to calculating $\beta$ becomes more complex. While Eq. (2a) still holds the resistance is now a function of a nonlinear analysis and the conversion from demand (D, L) to demand effect (force, moment) is also no longer linear. For an existing design we seek a modification to Eq. (1) to account for this effect:

$$\phi R_{sys} R_n \geq c\Sigma\gamma Q_n^* \tag{6}$$

Where $\phi$ and other variables are unchanged from before, but $R_{sys}$ accounts for the difference between component and (sub)system reliability. If failure of the component equates to failure of the system then $R_{sys} = 1$. If the system is "brittle" and system failure is generally weaker than the individual component (such as the classic linked chain that fails when the weakest link fails) then $R_{sys} < 1$, while if there is beneficial system effect, for example through load redistribution, then $R_{sys} > 1$. The simplest approach is to select an $R_{sys}$ and then use simulation to assess the statistics of the demand/capacity ($R/Q$) ratio for use in Eq. (2a).

This basic approach has been studied for floors framed with repetitively placed cold-formed steel joists (Chatterjee 2016; Chatterjee et al. 2017; Smith et al. 2016 and 2018). For this system $R_{sys}$ was found to be significantly greater than 1.0. A value of 1.25 was recommended from the analysis in Smith et al. (2018) where it was assumed that a the floor target reliability would be the same as the member component reliability ($\beta$=2.5). The source of the beneficial system effect included (a) excess component reliability through the use of the same member across the floor, (b) beneficial load re-distribution from joist-to-joist under overload conditions, (c) beneficial decreases in the variation of the strength due to a large number of inter-connections between joists and sheathing which braces the joists, and (d) benefits from spatial variation in the demands. Note, wood design also uses a repetitive member factor of 1.15, which corresponds to a 15% increase in capacity (ANSI and AWC 2012).

For metal buildings it is possible to imagine a complete system analysis-based approach for the entire building system and abandoning traditional component checks. This approach has been explored for steel building frames and racks (e.g., Buonopane and Schafer 2006, Zhang et al. 2018). While this is a promising long term approach, in the near term it is considered more likely that (a) only well-defined subsystems will leverage system reliability, and (b) component checks will remain. Thus, the notion of the component level system reliability effect of $R_{sys}$ in Eq. (6) is pursued here. For metal buildings, the roof purlin system is closest to the previously studied cold-formed steel framing floor system, and is thus selected for the small studies herein.

It is worth noting that expectations for the benefit of system reliability are lower for metal building systems than typical cold-formed steel framed building systems. Of the 4 system benefits observed in cold-formed steel floor systems, only two are likely for metal building roofs: beneficial load re-distribution, and spatial variations in the demands across the subsystem. Compared with cold-formed steel framed building roofs, metal building roof purlins have larger spacing, less and lighter inter-connects to sheathing, and are optimized member-by-member, bay-by-bay, across load cases in a manner not typical in cold-formed steel framing.

## 3.     ARCHETYPE METAL BUILDING

An archetype building was specifically designed for this study by an MBMA member (MBMA 2019). This archetype building is focused on the roof and diaphragm, frame members and lateral load resisting systems are not explicitly studied unless they have some effects, such as the strut forces in the roof.

The specifications of the archetype metal building are summarized below:
- The building is 100' (clear span) x 125' (length) x 20' (Eave) with 0.49:12 roof slope.
- Design loading is based on 2018 IBC, ASCE7-16, Risk Category II for the Washington DC geographical location.
- The frame spacing is 25 ft, and purlins are continuous (lapped connections) over 5 bays of 25 ft.
- The seismic force in the Washington DC area is SDC B, and it is all "R=3.0" systems for the moment and braced frames.
- The LRFD method is used in the design.
- The roofing is a standard Through-Fastened Roof (TFR., PanelRib), with self-drilling screws, over purlin spacing of 5 ft. Additional sub-purlins are placed in the corner zones for high wind uplift.

- Non-proprietary connections or clips are used.
- The longitudinal, lateral force resisting system is braced frames in two side-walls, and roof-truss diaphragm. All are designed as tension-only X-diagonals.
- Secondary framing, purlins, and girts are 8.5" deep Zee-sections, but with different thickness, as needed.
- Roof live, and snow load patterns are always applied as stand-alone loads in addition to dead loads (only). Pattern loads are not combined with wind, and seismic loads and the live load are applied as the uniform live load. The same assumption is true for the snow loads.
- End post spacing was increased slightly, to force wider strut space in the roof plane. As a result, there are 5 identical purlin lines between strut/collector lines.
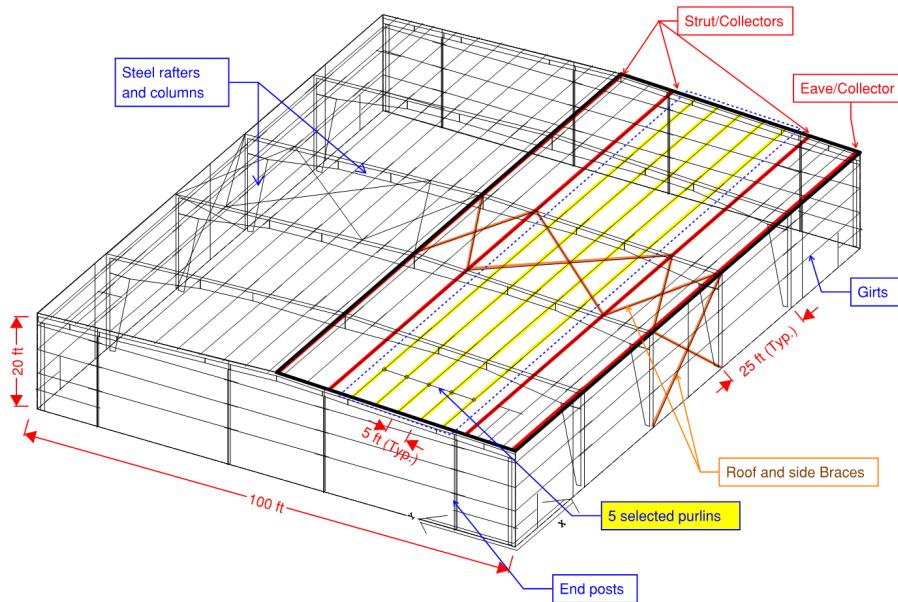


Figure 2: Archetype building (annotated)

Figure 2 shows the overall details of the archetype along with the designated area under study with five purlins. Although the loading is not precisely the same for the five selected purlins, as a common industry practice, the beam cross sections are assumed to be similar. The struts are not included in the roof sub-model to avoid complexities due to wind or seismic axial forces in these members.

Figure 3 summarizes all loading assumptions made by the designer and reflected in the calculation package. For more information on the archetype model, please see the Metal building archetype design (MBMA 2019).

**Calculations Package**

VP BUILDINGS
VARCO PRUDEN

**Bracing - Summary Report**

**Shape: ST2**
**Loads and Codes - Shape: ST2**
City:                                    County:                          State:                                Country:
Building Code: 2018 International Building Code                          Structural:    16AISC - LRFD        Rainfall: I: 2.00 inches per hour
Building Risk/Occupancy Category: II (Standard Occupancy Structure)      Cold Form:    16AISI - LRFD        f'c: 3000.00 psi Concrete

**Dead and Collateral Loads**                                                                                **Roof Live Load**
Collateral Gravity:3.00 psf            Roof Covering + Second. Dead Load: 2.02 psf                           Roof Live Load: 20.00 psf  Reducible
Collateral Uplift:  0.00 psf           Frame Weight (assumed for seismic):2.50 psf

**Wind Load**                          **Snow Load**                                        **Seismic Load**
Wind Speed: Vult: 111.00 (Vasd: 85.98) mph    Ground Snow Load: pg: 25.00 psf              Lateral Force Resisting Systems using Equivalent
                                                                                            Force Procedure
The 'Envelope Procedure' is Used       Flat Roof Snow: pf: 19.25 psf                        Mapped MCE Acceleration: Ss: 2.00 %g
Primaries Wind Exposure: C - Kz: 0.902  Design Snow (Sloped): ps: 19.25 psf                 Mapped MCE Acceleration: S1: 2.00 %g
Parts Wind Exposure Factor: 0.902      Rain Surcharge: 0.00                                 Site Class: Stiff soil (D) - Default
Wind Enclosure: Enclosed               Specified Minimum Roof Snow: 20.00 psf (Code)        Seismic Importance: Ie: 1.000
Topographic Factor: Kzt: 1.0000        Exposure Factor: 3 Sheltered - Ce: 1.10              Design Acceleration Parameter: Sds: 0.0213
Ground Elevation Factor: Ke: 1.0000    Snow Importance: Is: 1.000                           Design Acceleration Parameter: Sd1: 0.0320
                                        Thermal Factor: Heated - Ct: 1.00                    Seismic Design Category: A
NOT Windborne Debris Region            Ground / Roof Conversion: 0.70                       Seismic Snow Load: 0.00 psf
Base Elevation: 0/0/0                                                                        % Snow Used in Seismic: 0.00
Site Elevation: 0.0 ft                                                                       Diaphragm Condition: Flexible
Primary Zone Strip Width: 2a: 16/0/0                                                         Fundamental Period Height Used: 21/0/4
Parts / Portions Zone Strip Width: a: 12/0/0
Basic Wind Pressure: q: 24.18,(Parts) 24.18 psf                                             **Transverse Direction Parameters**
                                                                                            System NOT detailed for Seismic
                                                                                            Redundancy Factor: Rho: 1.00
                                                                                            Fundamental Period: Ta: 0.3201
                                                                                            R-Factor: 3.00
                                                                                            Overstrength Factor: Omega: 2.50
                                                                                            Deflection Amplification Factor: Cd: 3.00
                                                                                            Base Shear: V: 0.0100 x W

                                                                                            **Longitudinal Direction Parameters**
                                                                                            System NOT detailed for Seismic
                                                                                            Redundancy Factor: Rho: 1.00
                                                                                            Fundamental Period: Ta: 0.1963
                                                                                            R-Factor: 3.00
                                                                                            Overstrength Factor: Omega: 2.50
                                                                                            Deflection Amplification Factor: Cd: 3.00
                                                                                            Base Shear: V: 0.0100 x W

Figure 3: Loading assumption from the calculation package

## 4.    ROOF MODEL

The roof model in this study is a sub-model consisting of five purlins, along with cross-elements representing the decks and intermediate supports at the location of the frames. The numerical modeling has been performed in MASTAN 2, and the pre-processing and post-processing has been done via a MASTAN batch file in MATLAB to enable Monte Carlo (MC) simulations.

Figure 4 shows the geometry and boundary conditions of the purlin sub-assembly. In addition to the purlins, the steel decks passing over the purlins are also modeled to enable load redistribution between the purlins. As shown in Figure 5, the roof distributed loads are applied to the decks, and the decks are modeled as beam elements connected to the purlins to transfer the loads. The deck elements are assumed to behave elastically, and only the purlins have plastic hinges to enable plastic behavior and load redistribution in the analyses.

The "2nd-order Nonlinear" analysis module in MASTAN provides a load factor at which the displacements become very large, and the structure is thus unstable. The load factor is the reserve capacity of the system for the loads applied in the model. For an applied load, MASTAN's load factor can be understood as a resistance-to-demand factor.
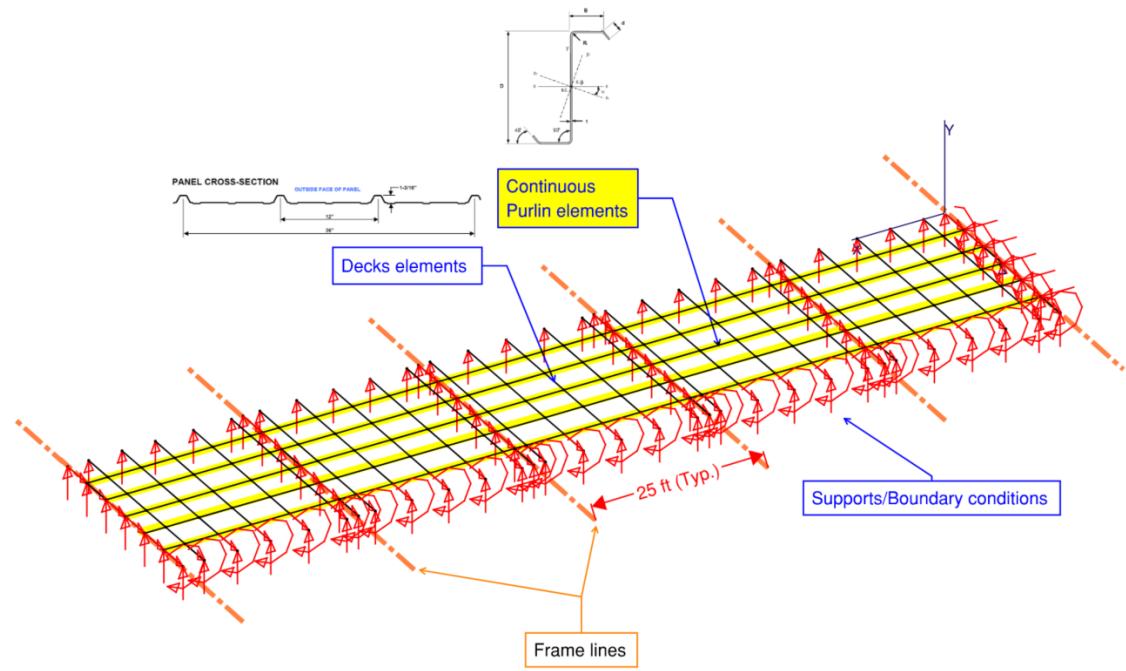
Figure 4: Geometry and boundary conditions of the purlin sub-assembly model
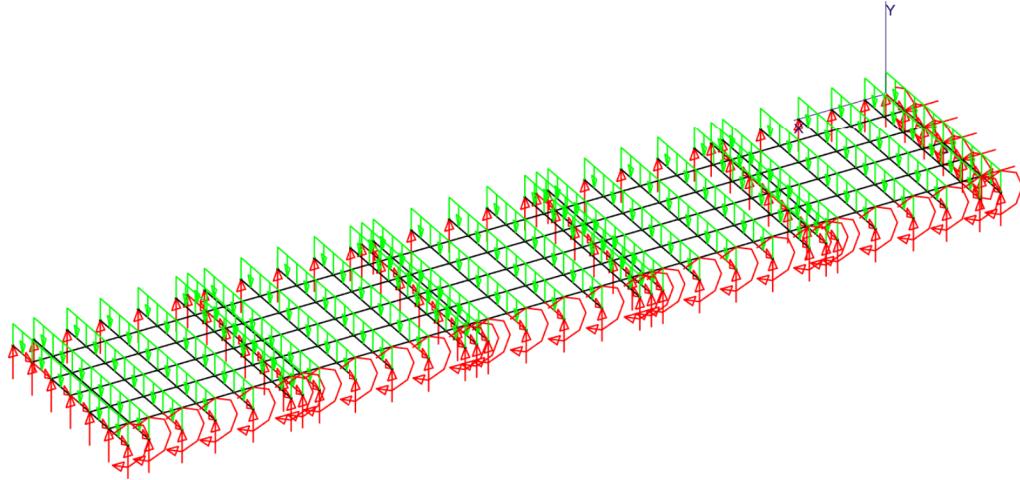


Figure 5: Beam loading via deck members

## 4.1 Purlin nominal capacity in the roof model

Figure 6 shows the purlin nominal flexural capacity along the length in positive and negative bending moments, extracted from the original beam design. The variable strength of the joist along the length is due to different unbraced lengths and different thicknesses of the purlin along the length as well as lapping of the individual purlins at supports.
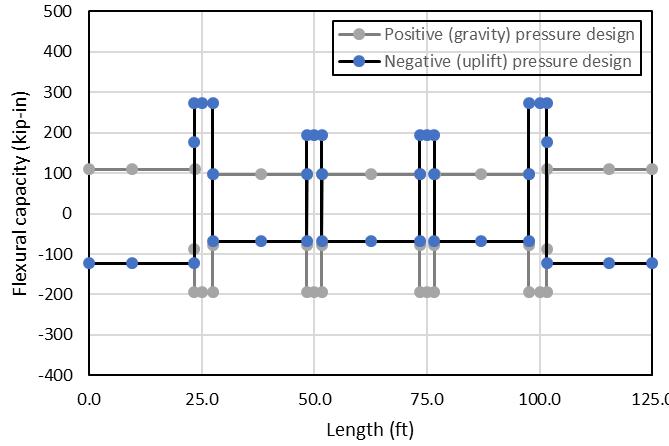
Figure 6: Purlin nominal flexural capacity along the length

## 4.2    load combinations

The controlling load combinations in the purlin design are summarized in Table 1.

Table 1: Design load combinations

| Positive (gravity) pressure design load combination | Load distribution |
|---|---|
| • Snow dominated: 1.2D+1.6PF2 (pattern2) | Partial load Full on 2 spans (LC9) |
| • Snow dominated:  1.2D+1.6PF2 (pattern3) | Partial load Full on 2 spans (LC10) |
| • Gravity dominated: 1.2D+1.6L+0.5W | Wind load, Pressure (LC19) |
| **Negative (uplift) pressure design load combination** | **Load distribution** |
| • Wind dominated: 0.9D-1.0W | Wind load, Suction (LC22) |

For the simulations we desire the mean demand, i.e. Eq. (4), not the nominal. The bias factors ($B$) are summarized in Meimand and Schafer (2014) and provided in Table 2(a). Accordingly, the load combinations in the analyses, including bias factors, are provided in Table 2(b).

Table 2: Mean load combination tables
(a) bias and variability from Meimand and Schafer (2014)

|  | Dead | Live | Wind | | Snow |
|---|---|---|---|---|---|
|  |  |  | 7-05 | 7-10 |  |
| $V_{Qi}$ | 0.1 | 0.25 | 0.37 | 0.37 | 0.26 |
| $B_i$ | 1.05 | 1.0 | 0.92 | 0.575 | 0.82 |

(b) resulting mean load combinations

| Positive (gravity) pressure unfactored load combination | Load distribution |
|---|---|
| • Snow dominated: 1.05D+0.82PF2 (pattern2) | Partial load Full on 2 spans (LCU9) |
| • Snow dominated:  1.05D+0.82PF2 (pattern3) | Partial load Full on 2 spans (LCU10) |
| • Gravity dominated: 1.05D+1.05L+0.575W | Wind load, Pressure, (LCU19) |
| **Negative (uplift) pressure unfactored load combination** | **Load distribution** |
| • Wind dominated: 1.05D-0.575W | Wind load, Suction, (LCU22) |

## 4.3　　　Resistance Variables

As shown in Figure 6, for positive and negative pressure design load combinations, the strength pattern along the length is different, due to different moment distributions and different unbraced lengths of the purlins in positive and negative pressures. The nominal flexural capacity along the length are extracted from the original beam design. While the distribution of the capacity is assumed to be deterministic, the purlin capacity in each bay and the connection region is assumed to be independent random variables with the capacity equal to the nominal capacity multiplied by material ($M_m$), fabrication ($F_m$), and professional factors ($P_m$), equal to 1.1, 1.0, and 1.0, respectively, per AISI S100 chapter K, for CFS joists. Accordingly, the mean capacity is 1.1 times the nominal capacity as follows:

$$R_m = M_m F_m P_m R_n \quad \text{or} \quad R_m = 1.1 R_n \tag{7}$$

The coefficient of variation (COV) is also calculated to be 0.15 ($V_R = 0.15$) per AISI-S100 chapter K, for CFS joists. $R_m$ and $V_R$ are used to generate random strength variables of each purlin along the length. The strength of adjacent purlins are assumed to be independent, and also the strength along the length of each purlin is independent, including the splice region.


## 4.4　　　Load Variables

The load pattern for all loads is taken as a deterministic input, but the load magnitudes for each bay and each joist are taken as an independent random variable. Load random variables for each load type are produced using the bias factor and a coefficient of variations in the literature, as described in the following sections.


### 4.4.1　　Dead and live loads

Dead and live loads are uniformly distributed loads, but to include the load variability, the load magnitude in the tributary area of each joist is assumed to be an independent random variable. For each analysis, the distributed gravity loads are taken from a pool of random variables generated with normal distribution. For dead loads, a bias factor and a coefficient of variations of 1.05 and 0.10, respectively, are considered per Meimand and Schafer (2014). For live loads, a bias factor and a coefficient of variations of 1.00 and 0.25, respectively, are used to generate Gaussian random variables.


### 4.4.2　　Snow load

Per design load combinations, the 2$^{nd}$ and 3$^{rd}$ bay of each joist gets 100% of the mean snow load, and the rest of the bays gets 50% of the mean snow load, as shown in Figure 7. For each analysis, there are a total of 5 independent random loads for each beam, for a total of 25 independent random loading variables. A bias factor and a coefficient of variations of 0.82 and 0.26, respectively, per Meimand and Schafer (2014), is used to generate random variables with a normal distribution.
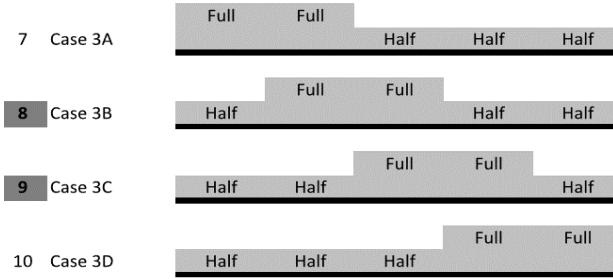
Figure 7: Snow load pattern

### 4.4.3 Wind load

The wind load pattern is taken per ASCE7-16 load patterns, as shown in Figure 8 (ASCE and SEI 2010). The wind load pattern is taken as a deterministic input, but the wind pressure magnitude in each bay is a random variable. The wind bias factor for ASCE7-10 is 0.575, and the coefficient of variation is 0.37 (Meimand and Schafer, 2014; ASCE and SEI 2010, 2016). It is assumed that ASCE7-16 has the same bias and standard deviation. For simplicity, the wind random variables are generated with a normal distribution.
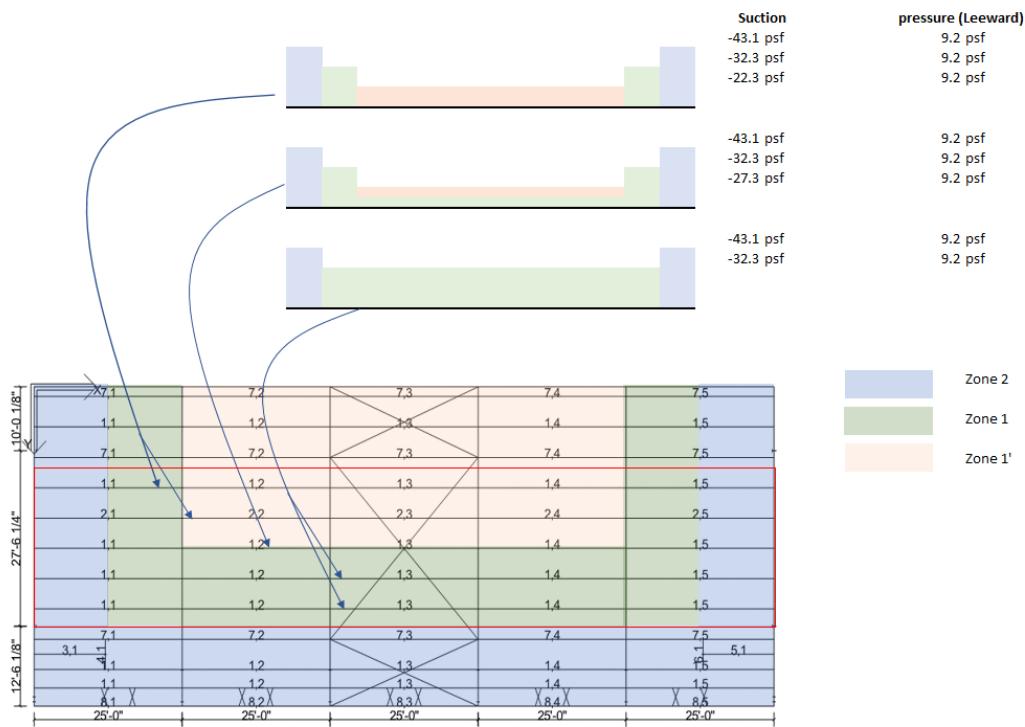


Figure 8: Wind load pattern and nominal magnitudes

### 4.4.4    Load summary

Figure 9 summarizes all the deterministic load patterns and magnitudes over the roof region under study. Figure 10 shows a single realization of the simulation for the same load patterns. All variables are generated with magnitudes following a normal distribution. As shown, the loading is variable for adjacent joists and along each joist. Each model in the MC analysis is subjected to a different realization of the random loads (similar to Figure 10) and averages across simulations converge to the original deterministic distributions (Figure 9).
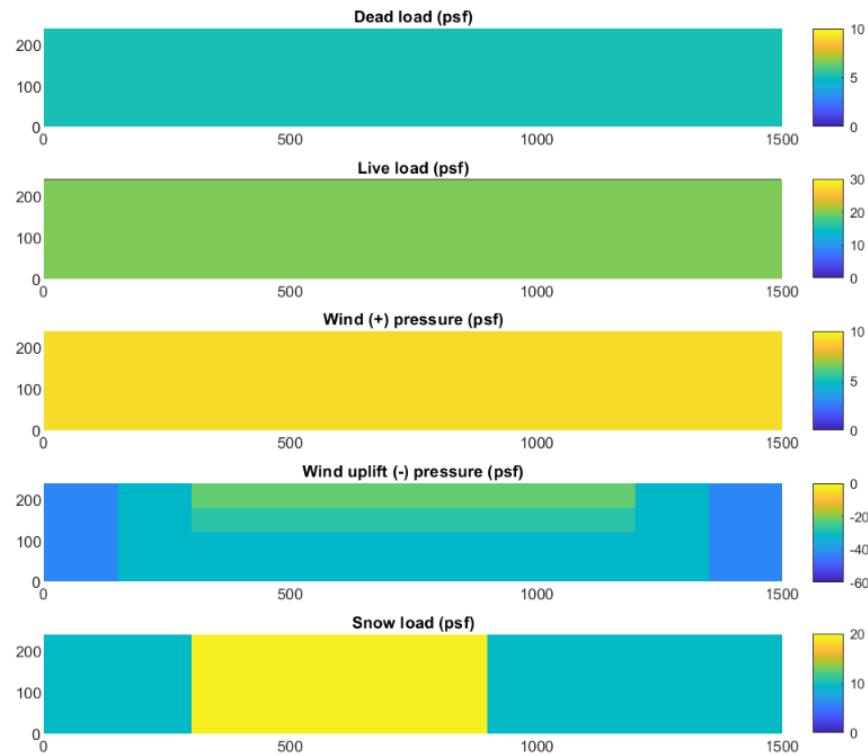


Figure 9: Deterministic load pattern and magnitudes (lengths are in inches)
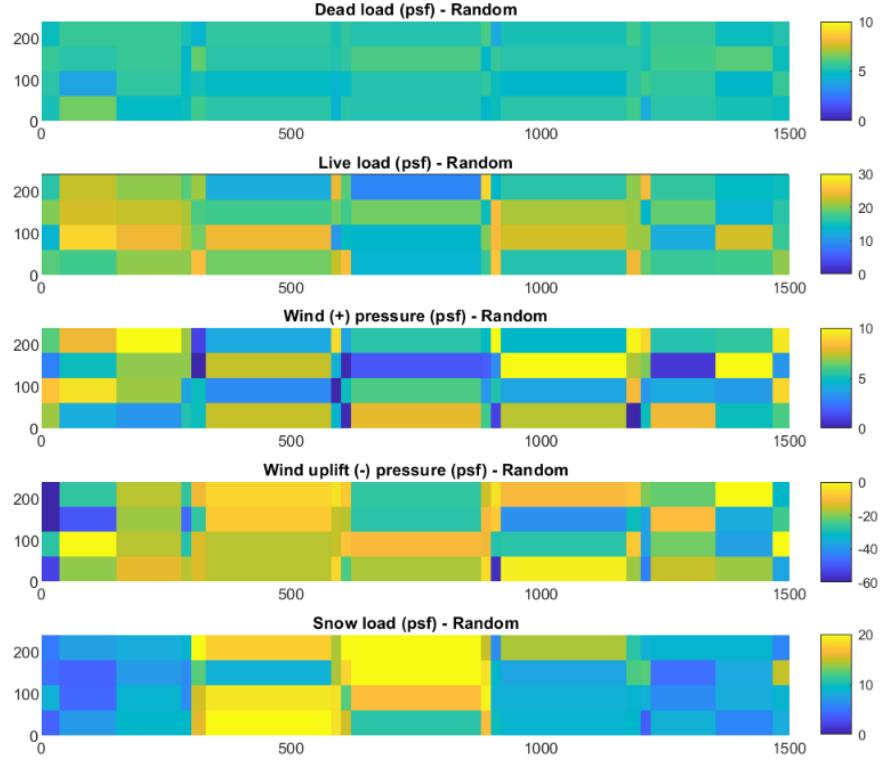
Figure 10: One realization of random load variables (lengths are in inches)

## 5.    RELIABILITY ANALYSIS APPROACH

As shown in Figure 1(a), the load effect, $Q$, and the resistance, $R$, are random variables and the probability of exceeding a limit state assuming a lognormal distribution shown in Figure 1(b) can be calculated as Eq. (2a), i.e.:

$$\beta = \frac{\ln\left(\frac{R}{Q}\right)_m}{\sigma_{\ln\left(\frac{R}{Q}\right)}}$$

(8)

where, $m$ refers to the mean and $\sigma$ the standard deviation of the natural log of the resistance-to-load $(R/Q)$ ratio. This study considers a direct approach in addressing the system reliability of the roof purlins. This approach can be summarized in the following main steps:

Step 1: Generate independent random variables for resistance $(R)$ of all purlins, including initial guess for $R_{sys}$

Step 2: Generate independent random variables for all applied loads $(Q)$

Step 3: Perform a series of $2^{nd}$-order nonlinear analyses and determine the $R/Q$ ratios (or load factor in MASTAN) at which collapse or other performance criteria is met

Step 4: Calculate $\ln\left(\frac{R}{Q}\right)_m$ and $\sigma_{\ln\left(\frac{R}{Q}\right)}$

Step 5: Calculate the reliability factor $\beta$ from Eq. (8)

Step 6: If $\beta > \beta_o$, (where $\beta_o$ = target reliability) increase $R_{sys}$ and go back to Step 1

To incorporate the system reliability effect on the member design, the initial $R_{sys}$ factor is assumed to be 1.0 and if the reliability index ($\beta$) is larger than the target reliability index (typically $\beta_o = 2.5$ for members and systems), then the whole loop can be repeated with slightly higher $R_{sys}$ (increments of 0.05) until the time $\beta$ is not smaller than the target reliability index, $\beta_o$. The number of random variable samples needs to be large enough to make sure the calculated logarithmic mean and logarithmic standard deviation of the results is stable with less than 1% error.

## 6.    SIMPLIFIED EXAMPLE

Before performing MC simulations, the merits of using the system reliability approach instead of the element reliability approach are studied using a simplified example as follows. Consider the following estimation of the reliability index for the roof under the uplift load combination. The applied load to the beam is an entirely uniform wind dominated unfactored load of 1.05D-0.575W. The load pattern is defined in Figure 9. The resistance of the purlins along the length is defined as 1.10 times the nominal capacity of the purlin as shown in Figure 5.

MASTAN 2nd-order nonlinear analysis has been performed, and the resistance-to-load ratio is calculated to be 2.561 at collapse, as shown in Figure 11. The figure shows the location of the plastic hinges and the load factor at which the plastic hinge formed. Accordingly, the reliability index can be approximated from Eq. (2b) and calculated using $V_Q = 0.31$ (Meimand and Schafer 2014), $\frac{R_m}{Q_m} = 2.561$, and $V_R = 0.15$:

$$\beta = \frac{\ln\left(\frac{R_m}{Q_m}\right)}{\sqrt{V_R^2 + V_Q^2}} = \frac{\ln(2.561)}{\sqrt{0.15^2 + 0.31^2}}$$

$$\beta = 2.73 > \beta_o = 2.5$$

The calculated system reliability index of 2.73 is larger than the target reliability index of 2.5, and therefore, it is expected that it may be possible to achieve a system reliability factor, $R_{sys}$, larger than 1.0. The $R_{sys}$ factor is determined in the following section using a large number of models in MC simulations.



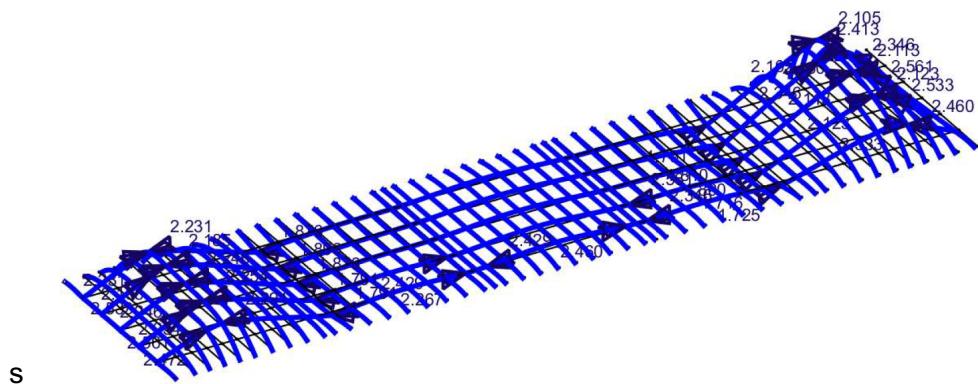**** Deflected Shape:  2nd-Order Inelastic, Incr # 44, Applied Load Ratio = 2.561 ***

Figure 11: Applied load ratio for the uplift load case

# 7.    MONTE CARLO SIMULATIONS

Monte Carlo simulations have been performed following the steps explained in Section 5. To determine the minimum number of models required to get a stable standard deviation (STD) or Coefficient of Variation (COV) of the $R/Q$ or load factors, a large number of simulations have been performed for one load combination and the results are shown in Figure 12. As shown, after about 100 simulations, COV and STD are stable and not changing with a higher number of simulations. To make sure that an adequate number of models are used in the simulations, a total of 200 simulations are considered for each load combination in the following.
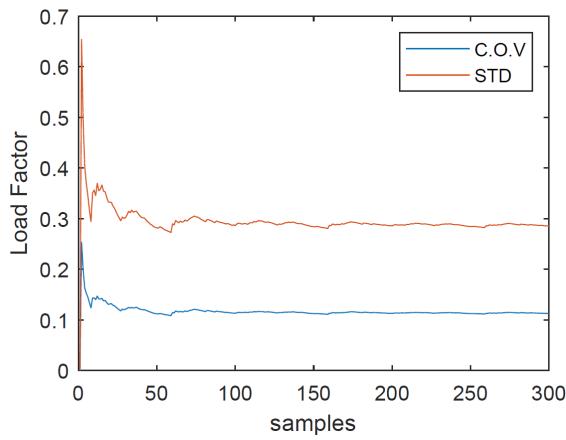


Figure 12: Standard deviation (STD) on and coefficient of variation (COV) convergence

Figure 13 shows the load factor ($R/Q$) distribution at collapse for different load cases and $R_{sys}$ factors, changing between 1.0 and 1.35, with no deflection limit state. As expected, the average $R/Q$ factors decrease as the $R_{sys}$ factor in increased. The histograms of the $R/Q$ distribution show less spread for the gravity dominated load case (1.2D+1.6L+0.5W) and more spread for snow and wind dominated load cases.

By assuming an equal likelihood of occurrence for each load combination, a combined $R/Q$ distribution is provided for each $R_{sys}$ factor, including all load combinations, as shown in Figure 14. The system reliability index, $\beta$, is calculated using Eq. (8). The logarithmic mean of the $R/Q$ ratio and the logarithmic standard deviation per each $R_{sys}$ factor is calculated based on the results of 800 simulations for a total of four load combinations.

The results in Figure 14 show that for $R_{sys}$=1.0, the system reliability index of 3.24 is significantly higher than the target reliability index of 2.5. This shows the potential merits of using the system reliability approach rather than the member reliability approach. By increasing $R_{sys}$ to 1.15, the reliability index is close to the target index of 2.5. It can be concluded that the strength of the purlins can be increased by 15% to account for the system reliability effect. As shown, design with a $R_{sys}$>1.15 results in failing to meet the target reliability index.

In the 2nd-order nonlinear simulations in MASTAN, there is a possibility that the model converges at extensive/unrealistic deformations. In these cases, it is required to limit the deformations to avoid unrealistic results. Accordingly, a deflection limit of L/40, which corresponds to about 1.25%

total plastic hinge rotation, is considered in Figures 14 and 15. The 1.25% total plastic hinge rotation is generally achievable for cold-formed steel members (Ayhan and Schafer 2017) but is not the focus of this study. As shown in Figure 15, the 15% increase in the purlin strength still provides a system reliability index of 2.51, which is more than the target reliability index.
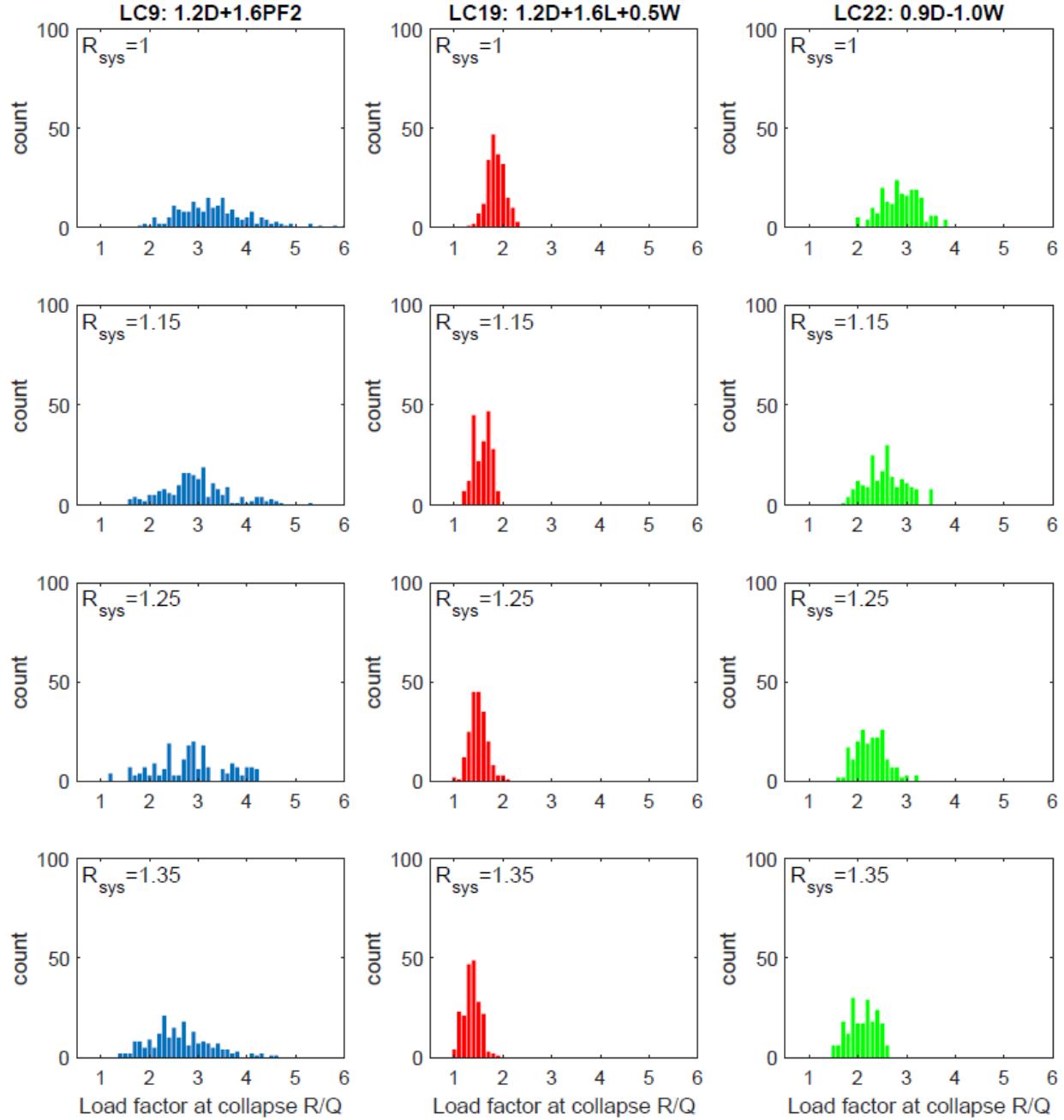


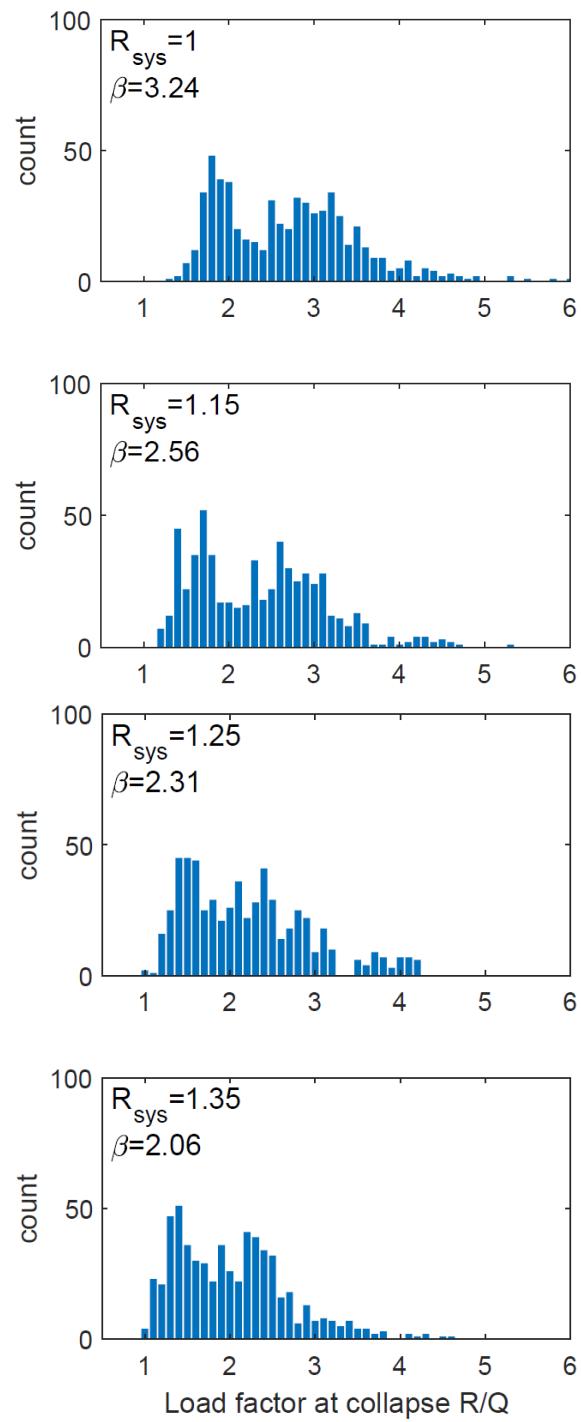Figure 13: "Load factor at collapse" distribution for different load cases and $R_{sys}$ values (no deflection limit)

Figure 14: Load factor at collapse distribution and system reliability index for different $R_{sys}$ values (no deflection limit)
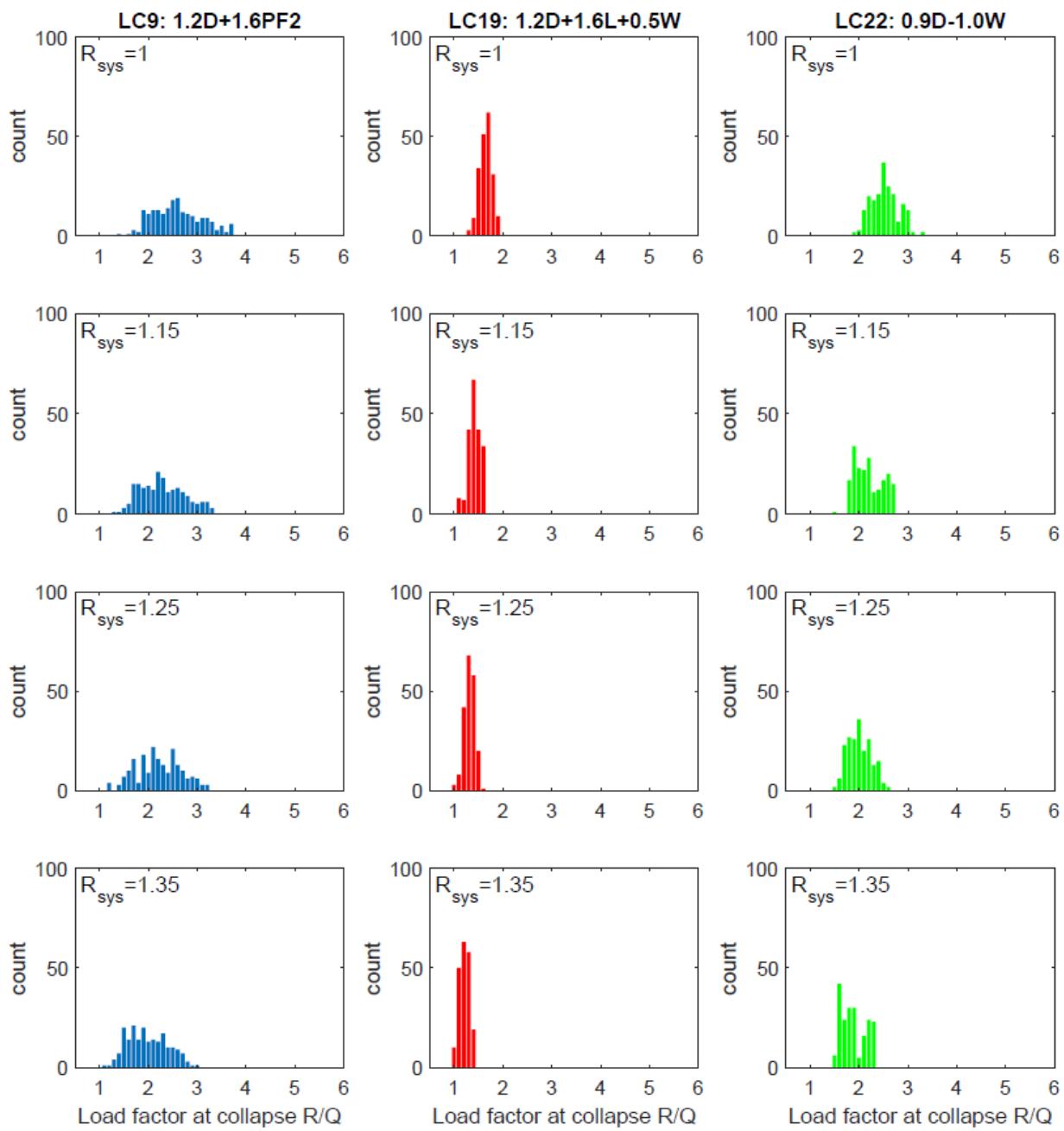
Figure 15: "Load factor at collapse" distribution for different load cases and $R_{sys}$ values (including deflection limit state of L/40)
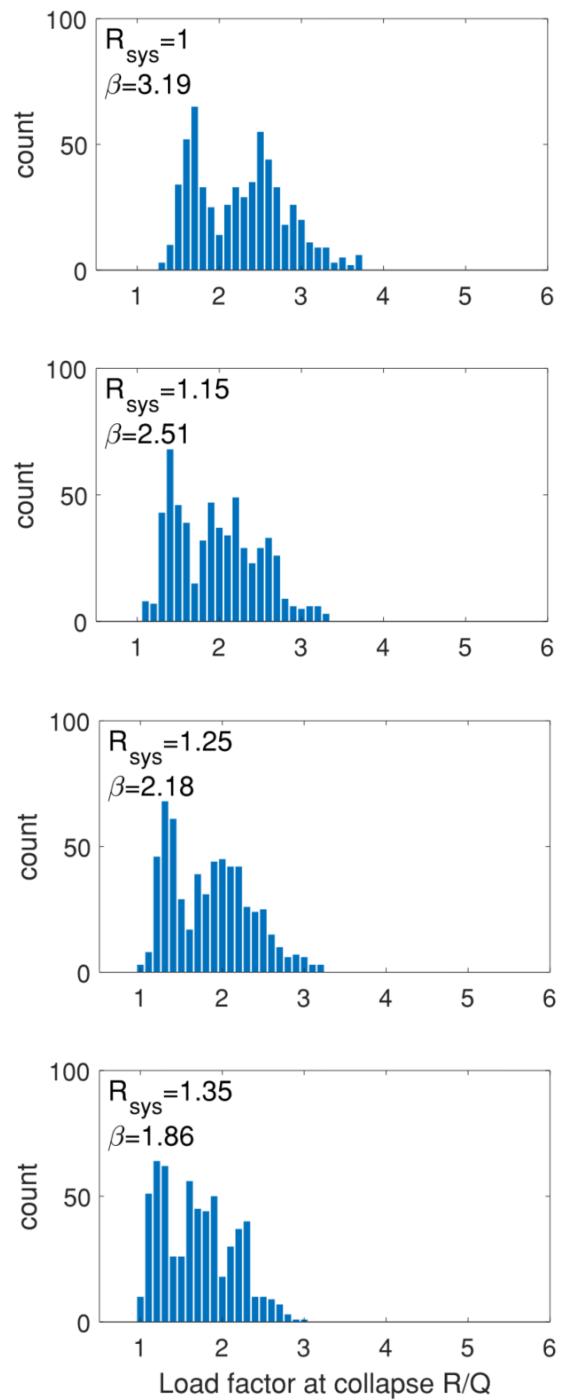
Figure 16: Load factor at collapse distribution and system reliability index for different $R_{sys}$ values (including deflection limit state of L/40)

## 8.      DISCUSSION

Adoption of an $R_{sys}$ factor for use in design would require careful definition of the "system" and ensuring that the system and its possibilities were faithfully represented in the analysis justifying the selected $R_{sys}$. The preliminary analysis provided herein suggests that even though metal building system purlins are highly optimized to existing load cases, and relatively sparsely spaced in the roof, it may be possible to benefit from system reliability.

The roof model employs plastic hinges for the purlins that assume elastic perfectly-plastic (EPP) response. Although total plastic rotations allowed are small, the EPP assumption is not strictly true. Further, the model does not capture out-of-plane demands that result as the purlins collapse and attempt to twist under load. Deck-to-purlin connections, which may limit the benefits of the deck under large deformations, are not considered in the developed model.

The use of independent random variables (even though mean-centered about the deterministic values) for the load magnitude may artificially increase the spatial variation. Correlated random variables or other more sophisticated treatments of the spatial load variation may be warranted.

The controlling load cases were down-selected from a large number of considered load cases through the use of conventional design. The impact of load cases not included in the final MC simulations remains unknown. Additional examination of the best methods to limit the number of considered load variations, but still capture the large number of load cases commonly considered in design, is needed.

The single system analysis approach of Section 6 provided estimated response similar to the more involved MC simulations with a single nominal collapse analysis. Suggesting that simpler means to utilize load redistribution may be possible. If a single nonlinear collapse analysis was completed for every load case this may be as useful as the MC simulations performed herein on a small number of load cases – further work in this regard is needed.

## 9.      SUMMARY AND CONCLUSIONS

This study has provided an analytical approach to incorporate system reliability effects in the design of roof purlins in metal buildings. It is intended to reflect the system effects in a component design factor, namely $R_{sys}$, that can be used to increase the design capacity of the purlins. Based on an archetype metal building design Monte Carlo simulations have been performed to study the reliability of a group of roof purlins connected via profiled steel decks. The geometric and material nonlinear collapse analyses of the roof segment have been performed in MASTAN to find the ultimate resistance-to-capacity ratios, and the results have been used to calculate the reliability index for a group of five purlins designed with different $R_{sys}$ factors. The results showed the beneficial effect of including system reliability effects in the design of the roof purlins. The $R_{sys}$ factor is estimated to be about 1.15, which means a 15% increase in the purlin capacity in design. A deflection limit of L/40 was considered in the simulations, which corresponds to about 1.25% total plastic hinge deformation at failure. More studies are required to establish a path to evaluate the rotational capacity of the purlins and incorporate the nonlinear behavior of the connecting steel decks into the simulations. The results provided here can be interpreted as a proof of concept for the effect of system reliability on the design of steel purlins, but more research is required to provide an $R_{sys}$ factor that reflects all characteristics of the actual roofing system.

## 10.    ACKNOWLEDGMENTS

## References

AISI-S100-16 (2016) North American Specification for the Design of Cold-Formed Steel Structural Members. American Iron and Steel Institute, Washington, DC ANSI/AISI-S100-16.

ANSI and AWC (American National Standards Institute and American Wood Council). (2012). "National design specifications for wood construction." ANSI/AWC NDS 2012, Leesburg, VA.

ASCE and SEI (Structural Engineering Institute). (2010). "Minimum design loads for buildings and other structures." ASCE/SEI 7-10, Reston, VA.

ASCE and SEI (Structural Engineering Institute). (2016). "Minimum design loads for buildings and other structures." ASCE/SEI 7-16, Reston, VA.

Ayhan, D., and Schafer, B. W. (2017). "Characterization of in-plane backbone response of cold-formed steel beams." J. Const. Steel Res., 132, 141–150.

Buonopane, S.G., Schafer, B.W. (2006). "Reliability Implications of Advanced Analysis in the Design of Steel Frames." ASCE, *Journal of Structural Engineering.* 132 (2) 267-276. (doi:10.1061/(ASCE)0733-9445(2006)132:2(267))

Chatterjee, A. (2016). "Structural system reliability with application to light steel-framed buildings." Ph.D. dissertation, Virginia Polytechnic Institute, Blacksburg, VA.

Chatterjee, A., Arwade, S. R., Schafer, B. W., and Moen, C. D. (2017). "System reliability of floor diaphragms framed from cold-formed steel with wood sheathing." J. Struct. Eng., 10.1061/(ASCE)ST.1943-541X.0001958, 04017208.

Meimand, V. Z., & Schafer, B. W. (2014). Impact of load combinations on structural reliability determined from testing cold-formed steel components. Structural safety, 48, 25-32.

MBMA (2019) Metal Building Archetype for Roof System Reliability Studies. (private communication)

Smith, B. H., Arwade, S. R., Schafer, B. W., and Moen, C. D. (2016). "Design component and system reliability in a low-rise cold-formed steel framed commercial building." Eng. Struct., 127, 434–446.

Smith, B. H., Chatterjee, A., Arwade, S. R., Moen, C. D., & Schafer, B. W. (2018). System Reliability Benefits of Repetitive Framing in Cold-Formed Steel Floor Systems. Journal of Structural Engineering, 144 (6) 04018061.

Zhang, H., Liu, H., Ellingwood, B.R., Rasmussen, K.J.R. (2018). "System Reliabilities of Planar Gravity Steel Frames Designed by the Inelastic Method in AISC 360-10." ASCE, J. of Struct. Eng. 144 (3) 04018011.